Optics and Lasers in Engineering 50 (2012) 231–235

Contents lists available at SciVerse ScienceDirect

Optics and Lasers in Engineering

journal homepage: www.elsevier.com/locate/optlaseng

Leaf cuticle topography retrieved by using fringe projection

Amalia Martínez [a], J.A. Rayas [a], Raúl R. Cordero [b,*], Daniela Balieiro [c,d], Fernando Labbe [e]

[a] Centro de Investigaciones en Óptica, Loma del Bosque 115, Col. Lomas del Campestre, León, Gto., México
[b] Universidad de Santiago de Chile, Ave. Bernardo O'Higgins 3363, Santiago, Chile
[c] Leibniz Universitaet Hannover, Herrenhauser Strasse 2, Hannover, Germany
[d] Pontificia Universidad Católica de Chile, Ave. Bernardo O'Higgins 340, Santiago, Chile
[e] Universidad Tecnica Federico Santa Maria, Ave. Espana 1680, Valparaiso, Chile

ARTICLE INFO

Article history:
Received 20 July 2011
Received in revised form
26 August 2011
Accepted 26 August 2011
Available online 14 September 2011

Keywords:
Fringe projection
Cuticle
Nondestructive testing

ABSTRACT

The combination (often referred to as phase-stepping profilometry, PSP) of the fringe projection technique and the phase-stepping method allowed us to retrieve topographic maps of cuticles isolated from the abaxial surface of leaves; these were in turn sampled from an apple tree (*Malus domestica*) of the variety Golden Delicious. The topographic maps enabled us to assess the natural features on the illuminated surface and also to detect the whole-field spatial variations in the thickness of the cuticle. Most of our attention was paid to retrieve the highly-resolved elevation information from the cuticle surface, which included the trace (in the order of tens of micrometers) left by ribs and veins. We expect that the PSP application for retrieving the cuticle topography will facilitate further studies on the dispersion and coverage of state-of-the-art agrochemical compounds meant to improve the defending properties of the cuticle. Methodological details are provided below.

1. Introduction

Non-destructive optical techniques can be used to retrieve shape as well as changes in shape due to, for example, out-of-plane deformation. Out-of-plane deformation is extensively monitored using interferometric techniques such as electronic speckle pattern shearing interferometry (ESPSI) [1–3], electronic speckle-pattern interferometry (ESPI) [4,5], and whole-field subtractive Moiré (WSM) [6,7]; using interferometers with out-of-plane sensitivity, ESPI and WSM have been also used to follow the thickness reduction associated with the strain localization onset [8,9]. However, the high sensitivity of the applied inteferometric techniques restricted these measurements such that shape changes only up to 10 μm could be measured.

Monitoring highly-resolved elevation information in the order of tens of micrometers requires applying whole-filed optical techniques of greater dynamical range than the interferometry-based methods, such as those based on the fringe projection technique [10–18]. As pointed out in [13], these techniques are often referred according to the particular fringe analysis method used in the measurement: phase stepping profilometry (PSP) [14,15], Fourier transform profilometry (FTP) [16], wavelet transform profilometry (WTP) [17], etc. In [18,19] a comparison is presented.

The fringe projection technique for contouring involves projecting gray-code straight fringes onto the surface of the specimen. The topography of the specimen leads to variations in the fringe pattern (captured using a camera), which are related to the actual shape of the specimen. The technique has been successfully applied to monitor changes in shape that involved out-of-plane deformations greater than 10 μm [20–23].

We used PSP (as indicated above, a combination of the fringe projection technique and the phase-stepping method) in order to retrieve the highly-resolved topographic maps of leaf cuticles. Fruits and aerial green parts of plants are protected by the cuticle [24–29]. The cuticular membrane (CM) is a non-cellular thin layer of polymer covering the outer cell layer; it consists of a matrix membrane (MX) made of polysaccharide microfibrils and lipophilic polymers and waxes. The cuticle is not only exposed to abiotic factors such as solar radiation, wind or rain, but it also interacts with microbes, fungi, and insects [24].

Attending to its importance as protective layer, there is great interest in the characterization of the cuticle as well as in the improvement of its defending properties using state-of-the-art agrochemical compounds; under water stress plants can close their stomata, but after taking such a measure, the loss of water of the plant is determined by the cuticle. Accordingly, efforts have been conducted on the assessment of the cuticular permeability to water and also on the development of cuticular antitranspirants [25]. However, further tests are needed in order to understand the

* Corresponding author.
E-mail addresses: amalia@cio.mx (A. Martínez), jrayas@cio.mx (J.A. Rayas), raul.cordero@usach.cl (R.R. Cordero), dbalieir@uc.cl (D. Balieiro), fernando.labbe@usm.cl (F. Labbe).

0143-8166/$ - see front matter © 2011 Elsevier Ltd. All rights reserved.
doi:10.1016/j.optlaseng.2011.08.011

Fig. 1. Veins and ribs may affect the dispersion and coverage of agrochemical compounds, when applied –as usually – by aspersion.

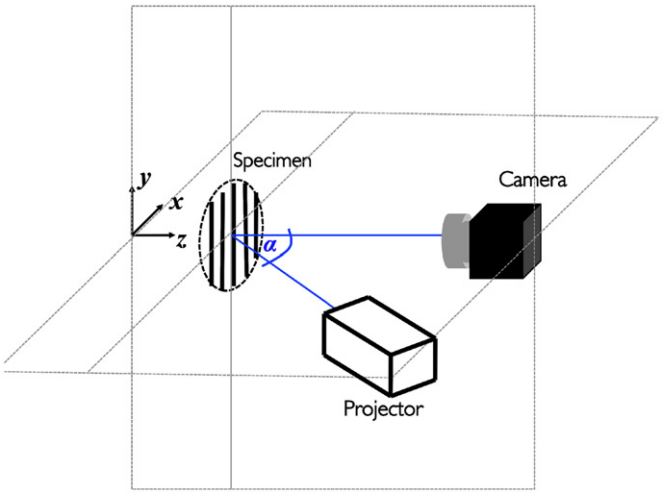

Fig. 2. Fringe projection optical setup.

mechanism of water diffusion through the MX, the differences (up to three orders of magnitude, see [26]) in the permeability of different species of plants, as well as the factors determining the performance of antitranspirant compounds (i.e. the compound dispersion and coverage). The cuticle topography is required in order to assess the effect of ribs and veins (see Fig. 1) on the compound dispersion and coverage.

As shown below, PSP allowed us to efficiently assess the natural features of cuticular membranes (CM) isolated from the abaxial surface of leaves; these were in turn sampled from an apple tree (*Malus domestica*) of the variety Golden Delicious. Our attention was mostly paid to assessing the highly-resolved elevation information from the cuticle surface, which included the trace left by ribs and veins. Also the whole-field spatial variations in the thickness of the tested specimens were measured.

2. Fringe projection

This technique for contouring involves projecting gray-code fringes onto the surface of the specimen and then viewing from another direction. Fig. 2 shows the required setup; a computer projector can be used as illuminating source. If the illumination distance is adequately large, the CCD camera in Fig. 2 captures, from the initially flat surface (meant to be a calibration surface), an intensity pattern I of nearly straight equally spaced fringes of period p

$$I(x,y)=A(x,y)+B(x,y)\cos\left(\frac{2\pi}{p}x+\theta(x,y)\right), \tag{1}$$

where A and B are the functions of position and θ is the modulation term related to perspective and optical aberration effects (see [30,31] for further discussions on the aberration dependence on the geometry of the object). If the illuminated specimen is not flat, its topography leads to the departure of the viewed fringes from straight lines such that a new intensity pattern I can be captured by the camera

$$I(x,y)=A(x,y)+B(x,y)\cos\left(\frac{2\pi}{p}x+\theta(x,y)+\phi(x,y)\right), \tag{2}$$

where ϕ is the phase modulation due to the topography of the illuminated specimen.

Note that the arguments $((2\pi/p)x+\theta(x,y))$ and $((2\pi/p)x+\theta(x,y)+\phi(x,y))$ in Eqs. (1) and (2), respectively, can be efficiently retrieved by applying the temporal phase-stepping method [32]. This involves capturing several fringe patterns generated at different times by shifting the phases in known amounts. This allows building up a set of simultaneous equations that are solved for the phase using algorithms [33–41]. Two popular algorithms that require a specific value of the phase shift are the *conventional* N-bucket [39] and the *self-calibrating* $(N+1)$-bucket [40]. In order to retrieve the arguments in Eqs. (1) and (2), we used in this work a 4-bucket algorithm [41].

The subtraction of arguments in Eqs. (1) and (2) allows isolating the phase modulation ϕ and canceling perspective and aberration effects. ϕ encodes information only on the elevation W (the departure of the specimen from a flat surface taken as a reference). According to [42,43], the phase modulation ϕ is related to the corresponding elevation W by

$$W(x,y)=\left(\frac{\phi(x,y)}{2\pi}\frac{p}{\tan\alpha}\right), \tag{3}$$

where α is the angle between the observation direction and the illumination direction.

Note that, when used to measure out-of-plane deformation, ϕ stands for the phase modulation induced between any pair of load stages. When the FTM is used to retrieve the phases at two load stages, the corresponding phase difference ϕ can be computed and then used (by applying Eq. (3)) to evaluate the out-of-plane *relative* displacement W between these two load stages. The fringe projection technique has been successfully applied to monitor changes in the shape that involved out-of-plane deformations greater than 10 μm [20–23].

3. Experimental details and data exploitation

We used phase-stepping profilometry, PSP (a combination of the fringe projection technique and the phase-stepping method) in order to retrieve the highly-resolved topographic maps of some cuticular membranes (CM).

The CM specimens that we tested were isolated using an aqueous solution containing enzymes; we selected the deciduous Apple tree (*Malus domestica*) cv. Golden Delicious due to the lack of trichoms and stomata on the abaxial leaf side. Disks of 20 mm diameter were punched out from mature leaves of field grown apple trees. The disks were vacuum infiltrated with an aqueous solution containing 0.2% (v/v) enzymes cellulase and 2% pectinase in 0.01 molar citric buffer, at pH 3 adjusted with KOH. Cuticles were kept in this solution for approximately 3 weeks. After that, cuticles from the upper astomatous leaf sides were collected. Isolated CM samples were washed in deionised water and then dried on teflon laminas using plastic tweezers. See [27–29] for

additional methodological details on the cuticle isolation. Fig. 3 shows isolated CM samples; the trace left by ribs and veins is apparent.

We used the optical experimental setup shown in Fig. 4. It includes a Dell digital projector of model WX 1609, 1280×800 pixels. The Pixelink CCD camera model PL-A741, 1280×1024 pixels. Note in Fig. 4 the rotating mount used to set the specimen.

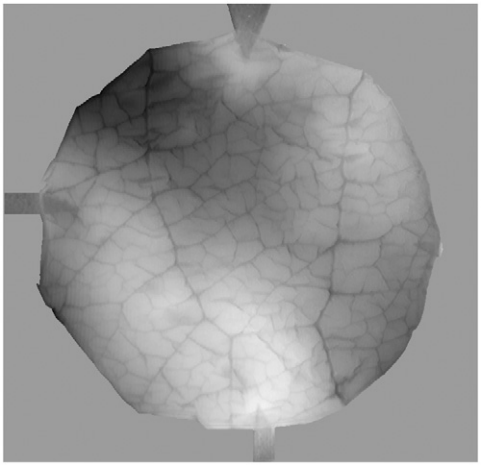

Fig. 3. Isolated leaf cuticle; the trace left by ribs and veins is apparent.

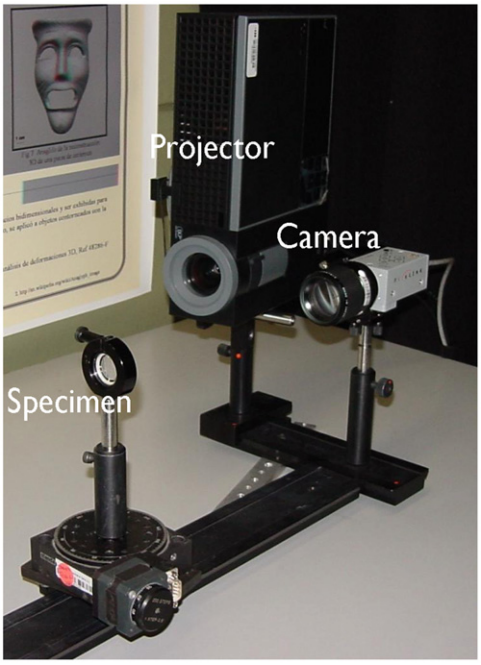

Fig. 4. Experimental setup. Note that the specimen is set on a rotating mount.

The projector allowed projecting gray-code fringes onto the surface of the specimen. α was equal to 25.6°. The illumination distance was selected adequately large, such that the CCD camera in Fig. 4 captured, when illuminating a flat surface, nearly straight equally spaced fringes of period $p=0.6$ mm. Instead, when illuminating a CM specimen, its topography led to the departure of the viewed fringes from straight lines (see Fig. 5a).

From the fringe pattern captured by the CCD, we retrieved the whole-field phase map using the phase-stepping method [32]. This involved capturing several fringe patterns, generated at different times by shifting the phases in known amounts. This allowed us to build up a set of simultaneous equations that were solved for the phase ϕ using the well known 4-bucket algorithm [41]. The latter is an arctangent function that at each pixel returns a principal value in the range $(-\pi,\pi)$ referred to as the *wrapped* phase. Fig. 5b shows the so-called wrapped map corresponding to the CM specimen shown in Fig 5a; this is an image built up by assigning a gray-scale value to each value in the range $(-\pi,\pi)$.

The *unwrapping* process implies adding to the *wrapped* value, the correct integral multiple of 2π [44]. Conventionally, one proceeds by calculating the difference between the wrapped phases at adjacent pixels along some chosen path. If this difference falls outside the range $(-\pi,\pi)$, it is assumed to be due to a 2π phase jump, which is then added or subtracted to one of the points in order to bring the difference between the phases back into the correct range [45]. In this way, an unwrapped phase map is obtained with neither discontinuities nor sign ambiguities. As shown in [41], noise is the main contributor to the phase-difference uncertainty. The noise influence in the phase-differences was reduced by applying a low-pass filter. Fig. 5c shows the so-called unwrapped map corresponding to the wrapped phase map shown in Fig. 5b; this is an image built up by assigning a gray-scale value to each value of ϕ.

Note that the 4-bucket algorithm renders the phase ϕ at each pixel. The phase depends on the intensity values captured using a CCD camera at each *step*. Therefore, the size of the set of discrete values of φ, which in turn determine the spatial resolution of the topographic maps, evidently depends on the camera resolution.

4. Results

Fig. 6 shows topographic maps of both the obverse (a) and reverse (b) side of a CM specimen. Note that plots in Fig. 6 do not stand for the actual shape of the illuminated sample but they show the elevation W relative to a flat surface taken as a reference.

The elevation W maps shown in Fig. 6 were both computed by applying Eq. (3); in the case of Fig. 6a, the whole-field ϕ values were calculated by subtracting the phase map corresponding to the obverse side of the specimen from the flat reference; in the case of Fig. 6b, the whole-field ϕ values were calculated by subtracting the phase map corresponding to the reverse side from the same flat reference. Both sides were found to have similar topography.

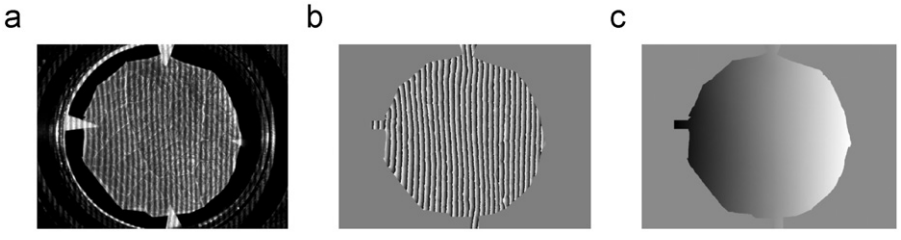

Fig. 5. (a) Gray-code fringes projected onto the surface of a CM specimen. (b) Wrapped phase map. (c) Unwrapped phase map.

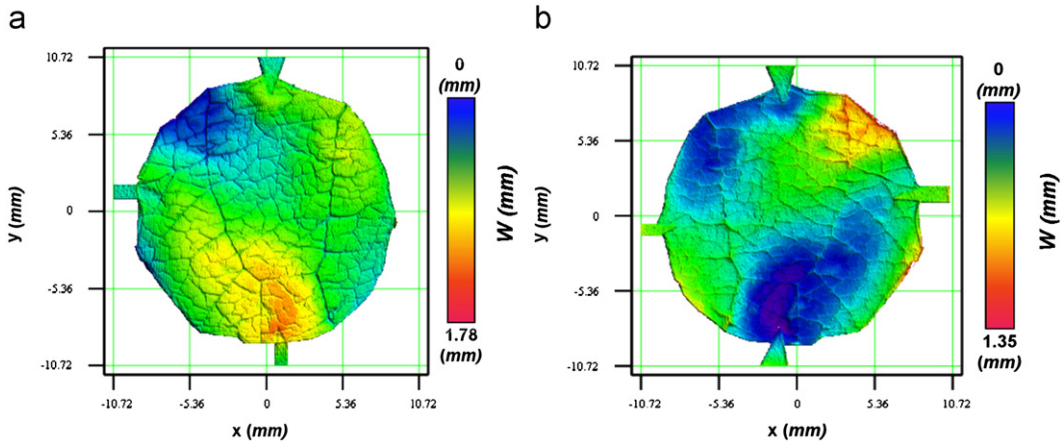

Fig. 6. Topographic maps of both the obverse (a) and reverse (b) side of a CM specimen. The elevation W (the departure of the specimen from a flat surface taken as a reference) was computed by applying Eq. (3) to the unwrapped phase values.

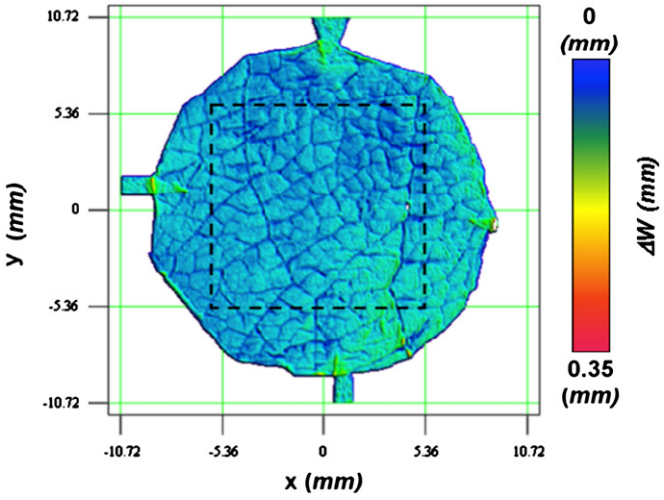

Fig. 7. Whole-field thickness values of a CM specimen. It was built up by subtracting the topography maps shown in Fig. 6. The average thickness within the area indicated by the dotted line was (130 ± 19) μm.

The topographic maps shown in Fig. 6 allowed us to retrieve the natural features from the cuticle surface, which included the trace left by ribs and veins. As expected, this trace was found to lead to variations in the elevation W in the order of tens of micrometers.

By subtracting the topography maps gathered from both sides of the tested specimens, we also assessed the whole-field spatial variations in the thickness of the tested specimens. Fig. 7 shows the whole-field thickness values of a CM specimen. This plot was built up by subtracting the topography maps shown in Fig. 6. Although the trace left by ribs and veins on the cuticular surface was expected to lead to significant spatial variations in the thickness, we found variations of only about 15% in the tested specimens. For example, the average thickness within the area indicated by the dotted line in Fig. 7 was (130 ± 19) μm.

5. Summary and conclusions

We used phase-stepping profilometry, PSP (a combination of the fringe projection technique and the phase-stepping method) in order to retrieve the highly-resolved topographic maps of some cuticular membranes (CM). The CM is a non-cellular thin layer of polymer covering the outer cell layer.

Attending to its importance as protective layer, there is great interest in the characterization of CM as well as in the improvement of its defending properties by using state-of-the-art agrochemical compounds; since these compounds are normally applied by aspersion, the CM topography is required in order to assess the effect of ribs and veins on the compound dispersion and coverage.

The cuticular membranes (CM) that we tested, were isolated from the abaxial surface of leaves; 20 mm diameter disks were sampled from field grown apple trees (*Malus domestica*) of the variety Golden Delicious. The isolation implied infiltrating the samples using an aqueous solution containing enzymes. After 3 weeks, isolated CM specimens were washed in deionised water and then dried on teflon laminas using plastic tweezers.

The elevation information was gathered from the surface of CM specimens by applying the fringe projection technique. It implied projecting gray-code straight fringes onto the specimen. The topography of the illuminated sample led to the departure of the viewed fringes from straight lines; the phase retrieved from that fringe pattern, ϕ, encoded information on the elevation W (the departure of the specimen from a flat reference). In order to retrieve the whole-field phase values we applied the temporal phase-stepping method with a 4-bucket algorithm.

As shown above, the combination of the fringe projection technique and the phase-stepping method allowed us to efficiently assess the natural features of the tested CM specimens. Our attention was mostly paid to retrieve the highly-resolved elevation information from the cuticle surface, which included the trace left by ribs and veins. This trace was found to be in the order of tens of micrometers. By subtracting the topography maps gathered from both sides of the tested specimens, we also assessed the whole-field spatial variations in the thickness of the tested specimens.

We expect that the PSP application for retrieving the cuticle topography will facilitate further studies on the effect of ribs and veins on the dispersion and coverage of state-of-the-art agrochemical compounds. Moreover, since thickness may have an effect on the cuticular permeability, we argue that the assessment of the whole-field spatial variations in the cuticular thickness may help to better understand the mechanism of water diffusion through the cuticle.

Acknowledgments

The support of CONICYT-CONACYT (Preis 2009–090), CONICYT-ANILLOS (Preis ACT98 and Preis ACT95), FONDECYT (Preis 1090471),

USACH-DICYT (Preis 041031-cc) and UTFSM-DGIP (Preis 251125) and is gratefully acknowledged.

References

[1] Patorski K. Digital in-plane electronic speckle pattern shearing interferometry. Opt Eng 1997;36:2010–5.
[2] Aebischer HA, Waldner S. Strain distributions made visible with image-shearing speckle pattern interferometry. Opt Lasers Eng 1997;26:407–20.
[3] Labbé F, Cordero RR, Martínez A, Rodriguez-Vera R. Measuring displacement derivatives by electronic speckle pattern shearing interferometry (ESPSI). Meas Sci Technol 2005;16:1677–83.
[4] Rastogi PK, Jacquot P, Pflug L. Holographic interferometry at LSA: some selected examples of its application. Opt Lasers Eng 1990;13:67–77.
[5] Martinez A, Rodriguez-Vera R, Rayas J, Puga H. Fracture detection by grating moire and in plane ESPI techniques. Opt Lasers Eng 2003;39:525–36.
[6] Han B, Post D, Ifju P. Moiré interferometry for engineering mechanics: current practices and future developments. J Strain Anal 2001;36:101–17.
[7] Post D, Han B, Ifju P. High sensitivity moiré: experimental analysis for mechanics and materials. New York: Springer-Verlag; 1994.
[8] Cordero RR, Labbé F. Measuring out-of-plane displacements by electronic speckle-pattern interferometry (ESPI) and whole-field subtractive moiré. Meas Sci Technol 2006;17:825–30.
[9] Labbé F, Cordero RR. Detecting the beginning of the shear band formation in uniaxial tensile tests by out-of-plane displacement measurements. Opt Lasers Eng 2007;45:153–9.
[10] Gai S, Da F. A novel fringe adaptation method for digital projector. Opt Lasers Eng 2011;49(4):547–52.
[11] Lei S, Zhang S. Digital sinusoidal fringe pattern generation: defocusing binary patterns VS focusing sinusoidal patterns. Opt Lasers Eng 2010;48(5):561–9.
[12] Wang Z, Nguyen DA, Barnes JC. Some practical considerations in fringe projection profilometry. Opt Lasers Eng 2010;48(2):218–25.
[13] Gorthi SS, Rastogi P. Fringe projection techniques: whither we are? Opt Lasers Eng 2010;48(2):133–40.
[14] Chen LC, Liao CC. Calibration of 3D surface profilometry using digital fringe projection. Meas Sci Technol 2005;16:1554–66.
[15] Zhang S. Recent progresses on real-time 3D shape measurement using digital fringe projection techniques. Opt Lasers Eng 2010;48(2):149–58.
[16] Su X, Zhang Q. Dynamic 3-D shape measurement method: a review. Opt Lasers Eng 2010;48(2):191–204.
[17] Zhong J, Weng J. Spatial carrier-fringe pattern analysis by means of wavelet transform: wavelet transform profilometry. Appl Opt 2004;43(26):4993–8.
[18] Quan C, Chen W, Tay CJ. Phase-retrieval techniques in fringe-projection profilometry. Opt Lasers Eng 2010;48(2):235–43.
[19] Huang L, Kemao Q, Pan B, Asundi AK. Comparison of Fourier transform, windowed Fourier transform, and wavelet transform methods for phase extraction from a single fringe pattern in fringe projection profilometry. Opt Lasers Eng 2010;48(2):141–8.
[20] Barrientos B, Cywiak M, Lee WK, Bryanston-Cross P. Measurement of dynamic deformation using a superimposed grating. Rev Mex Fis 2004;50:12–8.
[21] Tay CJ, Quan C, Wu T, Huang YH. Integrated method for 3-D rigid-body displacement measurement using fringe projection. Opt Eng 2004;43:1152–9.
[22] Quan C, Tay CJ, Huang YH. 3-D deformation measurement using fringe projection and digital image correlation. Optik 2004;115(4):164–8.
[23] Barrientos B, Moore AJ, Perez-Lopez C, Wang L, Schudi T. Three-dimensional displacement fields measured in a deforming granular-media surface by combined fringe projection and speckle photography. Opt Eng 1999;38:2069–74.
[24] Jeffree CE. The fine structure of the plant cuticle. In: Riederer M, Muller C, editors. Biology of the plant cuticle: annual plant review, 23. UK: Blackwell Publishing Ltd; 2006. p. 11–125.
[25] Iriti M, Picchi V, Rossoni M, Gomarasca S, Ludwig N, Gargano M, et al. Chitosan antitranspirant activity is due to abscisic acid-dependent stomatal closure. Environ Exp Bot 2009;66(3):493–500.
[26] Rieder M, Schreiber L. Protecting against water loss: analysis of the barrier properties of plant cuticles. J Exp Bot 2001;52:2023–32.
[27] Baur P. Lognormal distribution of water permeability and organic solute mobility in plant cuticles. Plant, Cell Environ 1997;20:167–77.
[28] Baur P. Mechanistic aspects of foliar penetration of agrochemicals and the effect of adjuvants. Recent research developments in agricultural & food chemistry, vol. 2; 1998 (pp. 809–837).
[29] Lopez-Casado G, Matas AT, Dominguez E, Cuartero J, Heredia A. Biomechanics of isolated tomato fruit cuticles: the role of the cutin matrix and polysaccharides. J Exp Bot 2007;58(14):3875–83.
[30] Fagg AH, Hales BS, Stahl HP. Systematic errors of a projection-moire contouring system. Proc SPIE 1992;1776:120.
[31] Zappa E, Busca G, Sala P. Innovative calibration technique for fringe projection based 3D scanner. Opt Lasers Eng 2011;49(3):331–40.
[32] Cloud G. Optical method in engineering analysis. Cambridge: University Press; 1995.
[33] Creath K. Phase Measurement Interferometry Techniques. Prog Opt 1998;26:350–93.
[34] Stahl HP. Review of phase-measuring interferometry in optical 29 and metrology III: recent advances in industrial optical inspection. In: Grover CP, editor. Proc SPIE 1991; 1332:704–719.
[35] Tiziani HJ. Optical methods for precision measurements. Opt Quantum Electron 1989;21:253–82.
[36] Carré P. Installation et Utilisation du Comparateur Photoélectrique et Interférentiel du Bureau International des Poids et Mesures. Metrologia 1996;2(1):13–23.
[37] Schwider J, Burow R, Elssner KE, Grzanna J, Spolaczyk R, Merkel K. Digital wave-front measuring interferometry: some systematic error sources. Appl Opt 1983;22:3421.
[38] Novak J. Five-step phase-shifting algorithms with unknown values of phase shift. Optik —Int J Light Electron Opt 2003;114(2):63–8.
[39] Huntley JM. In: Rastogi PK, editor. Digital speckle pattern interferometry and related techniques. Chichester: John Wiley; 2001.
[40] Surrel Y. Phase stepping: a new self-calibrating algorithm. Appl Opt 1993;32:3598.
[41] Cordero RR, Molimard J, Martinez A, Labbe F. Uncertainty analysis of temporal phase-stepping algorithms for interferometry. Opt Commun 2007;275:144–55.
[42] Barrientos B, Cerca M, Garcıa-Marquez J, Hernandez-Bernal C. Three-dimensional displacement fields measured in a deforming granular-media surface by combined fringe projection and speckle photography. J Opt A: Pure Appl Opt 2008;10:104027 (10 pp.).
[43] Gasvik KJ. Optical metrology. 3rd edn Chichester: Wiley; 2003.
[44] Ghigia DC, Pritt MD. Two-dimensional phase unwrapping theory, algorithm, and software. New York: John Wiley; 1998.
[45] Cordero RR, Molimard J, Labbe F, Martinez A. Strain maps obtained by phase-shifting interferometry: an uncertainty analysis. Opt Commun 2008;281:2195–206.